

Highly Improved Fabrication of Ag and Al Nanostructures for UV and Nonlinear Plasmonics

Krishnan Thyagarajan, Christian Santschi,* Philippe Langlet, and Olivier J. F. Martin

Plasmonics is the study of the collective oscillations of free electrons in metals that can be resonantly excited at optical frequencies. These oscillations exhibit unique optical properties across the electromagnetic spectrum and have been extensively studied for their ability to generate hot spots – regions where the incident field is enhanced by several orders of magnitude.^[1] Optical properties of such excitations have been exploited in the visible and the infrared parts of the electromagnetic spectrum.^[2] Apart from understanding fundamental light–matter interaction,^[3] applications include lasers,^[4] biochemical sensing platforms,^[5] biomedical therapeutics,^[6] optical trapping,^[7] and photodetectors.^[8] The high field enhancements have also attracted an interest in the field of nonlinear plasmonics, which requires such strong optical fields.^[9] Different nonlinear optical phenomena such as second harmonic generation (SHG),^[10] chirality,^[11] multiphoton luminescence,^[12] third harmonic generation,^[13] higher harmonic generation,^[14] ultrafast dynamics,^[15] and four wave mixing^[16] have been reported in recent studies. The most common femtosecond laser source used for nonlinear optical measurements in such experiments is a Ti:Sapphire laser, which operates best at $\lambda = 800$ nm. This implies for example that for SHG measurements the second harmonic corresponds to a wavelength of $\lambda = 400$ nm and for higher harmonics, it corresponds to even shorter wavelengths. This restricts the metals that can be used for such studies; especially for gold—the favorite plasmonic metal—in which interband transitions for wavelengths shorter than $\lambda = 500$ nm produce very significant losses.^[2] With the increasing interest in nonlinear plasmonics,^[17] the nanofabrication of metals that can work below $\lambda = 500$ nm needs to be mastered. Furthermore, UV plasmonics is another field of research which is becoming an active topic of study.^[18] The potential applications of UV plasmonics include surface enhanced Raman spectroscopy,^[19] enhanced down conversion of UV light,^[20] deep UV resonances,^[21] photodetectors,^[22] hyperbolic metamaterials,^[23] artificial colors,^[24] and plasmonic deep UV nanolithography.^[25]

Aluminum and silver fall into this category of plasmonic materials for both nonlinear optical as well as UV plasmonic

applications.^[12,26] Unfortunately, there exists great difficulty in nanofabrication with these metals due to their tendency to nucleate heterogeneously at multiple sites in the early stage of growth. This prevents not only a smooth surface but also causes large grain sizes leading to deformed shapes and lack of reproducibility for features (e.g., nanogaps) down to 10 nm.^[27] Different wetting layers, including Ge, Cu, and Ni have been shown to significantly improve the nanofabrication of Ag thin films.^[28] In this Communication, we focus on the fabrication of multiple pieces nanostructures; Scanning electron microscopy (SEM) images of fabricated silver and aluminum nanostructures of poor quality using a nonoptimized nanofabrication technique are shown in **Figure 1**. One can clearly see the poor surface quality, large grain size, and other unusual effects such as bridging between two adjacent plasmonic units. With the improvement in electron beam lithography techniques, the bottle neck in ultrasmall metallic nanostructure fabrication, especially for liftoff processes, shifts more and more to the quality of the deposited metal. Therefore improving the metal growth for lithographically defined nanostructures is crucial. Here, we show that the properties of the metal/oxide interface are of great importance and can drastically impact the fabrication outcome. Particularly the interfacial free energy γ plays a crucial role in the competition between creation of a continuous film and nucleation.^[42] Poor wetting and therefore nucleation occurs when the interfacial metal to oxide free energy $\gamma_{m/o}$ exceeds the difference of the interfacial energies between oxide $\gamma_{o/v}$ and metal $\gamma_{m/v}$ toward vacuum^[29]

$$\gamma_{m/o} > \gamma_{o/v} - \gamma_{m/v} \quad (1)$$

According to Equation (1) surface activation of the oxide layer, resulting in a higher interfacial free energy, facilitates wetting at an early deposition stage and, hence, can improve the quality of the metallic deposits. Some metal oxides, such as silver oxide are unstable when heated even to relatively low temperatures, releasing oxygen temporarily. The reaction of silver with O_2 is reversible. Consequently, at low O_2 pressure, dissociation of Ag_2O takes place to establish equilibrium,^[30] leading to an activated layer forming an energetically favorable surface for incoming silver. This phenomenon, which is reminiscent of oxygen gettering,^[31,32] can be exploited during the process of metal evaporation of silver onto the wafer.

Experimental Section

With this in mind, the nanofabrication of silver plasmonic nanostructures started with the spin-coating of a bilayer of electron

Dr. K. Thyagarajan, Dr. Ch. Santschi, Prof. O. J. F. Martin
Nanophotonics and Metrology Laboratory (NAM)
Swiss Federal Institute of Technology Lausanne (EPFL)
Station 11, CH – 1015 Lausanne, Switzerland
E-mail: christian.santschi@epfl.ch



Dr. P. Langlet
Center for Micro- and Nanotechnology (CMi)
Swiss Federal Institute of Technology Lausanne (EPFL)
CH – 1015 Lausanne, Switzerland

DOI: 10.1002/adom.201500740

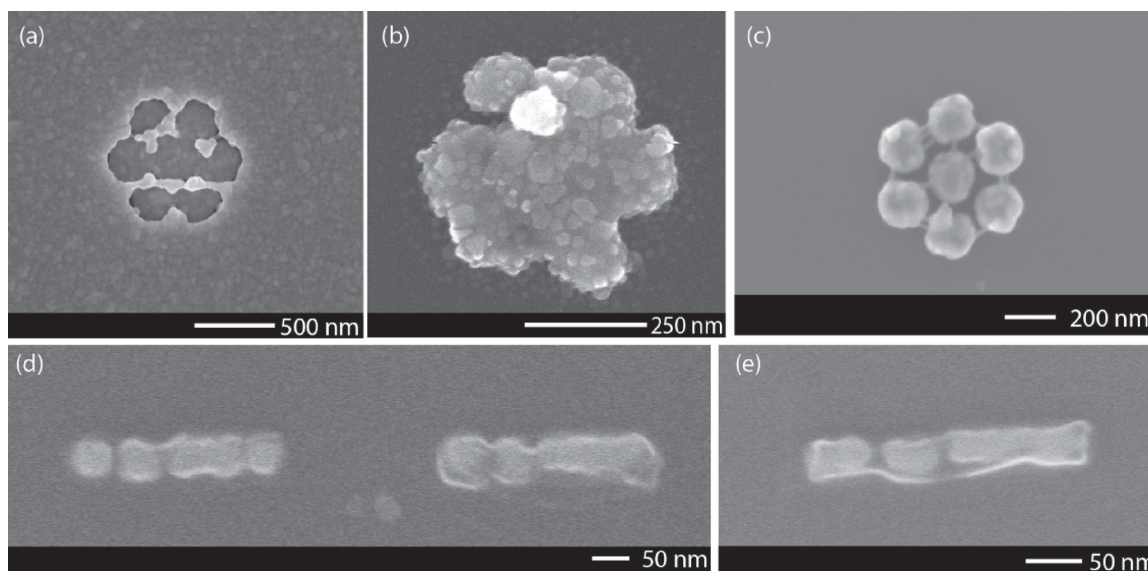


Figure 1. SEM images of the poor initial quality of a–c) silver and d,e) aluminum structures showing large surface roughness, large grain size, bridging between structures and poor adhesion to the substrate.

beam resist, consisting of polymethyl methacrylate (PMMA, obtained from Microresist Technology GmbH) with a mass of 495 kDa (thickness 120 nm) followed by a layer of 950 kDa (thickness 60 nm), onto a glass wafer. Compared to a single layer resist, this bilayer produced a very fine undercut, permitting lithographic features as small as 10 nm. After a chromium layer coating of 20 nm was evaporated on the resist for the need of a conductive layer during electron beam exposure, the required pattern was written onto the resists using electron beam lithography (Vistec EBPG5000 system) with a 100 keV electron beam (current 200 pA). A subsequent chromium etching followed by development in a mixture of MiBK solution and isopropyl alcohol was undertaken. As a first important step to assist in the surface activation, the developed wafer was subjected to oxygen plasma for about 15 s (O_2 : 300 sccm, RF power: 1 kW, pressure: 0.7 Torr, Oxford PRS900 dry etcher). This, additionally, allowed residual resist that is still in the gaps to come off and at the same time removed any major contaminants on the surface that might make it inert, thereby activating the surface. This step when carried out just before e-beam evaporation of metal ensured a much more uniform and controlled thin film deposition. For the metal evaporation step, first a 1 nm layer of silver was evaporated onto the wafer in presence of molecular oxygen resulting in a thin layer of silver oxide (O_2 : 10 sccm, pressure: 7.2×10^{-5} mbar, Leybold Optics LAB 600H evaporator). The chamber was then pumped out to 1×10^{-6} mbar; as mentioned above, this caused the oxygen from the thin oxide layer to depart, leaving a highly activated silver surface. Immediately afterward, the remaining amount of desired silver was evaporated onto the wafer at 4 \AA s^{-1} . This deposition of the remaining silver was done in three deposition steps, interrupting the process twice for 550 s to let the substrate cool down. After the evaporation, a liftoff carried out in acetone ensured that only the silver in contact with the substrate remains on the wafer. Usually, a thin adhesion layer of chromium or titanium is evaporated while depositing the metal. However, in this recipe, this adhesion layer is not necessary since the adhesion of the structures onto the wafer was observed to be good even without this extra layer. The entire fabrication process is shown as a schematic in **Figure 2a–h**. For this work, silver heptamers were fabricated due to their interesting nonlinear optical properties.^[32] SEM images of the dramatically improved features of the fabricated silver nanostructures and the quality of the silver surface can be seen in **Figure 2i,j**. Optical scattering measurements carried out on the structures (Olympus IX71 with 60 \times , 0.7 NA objective) are shown in **Figure 2k**. The good match between simulation and experiment shows the high quality of the fabricated silver nanostructures. The simulations

were carried out using the surface integral equation formalism with the substrate taken into consideration.^[33] The optical parameters were taken from the literature.^[34] To verify the chemical composition of the metal film constituting the structures, X-ray photoelectron spectroscopy (XPS) measurements were carried out. The measurements as seen in **Figure 2l** show that there is a very small percentage of oxygen still present in the structure and it is evenly spread throughout. This indicates a smooth quality of the evaporated film which thus results in good optical properties.

For nonlinear plasmonics, it is also important to improve the nanofabrication of aluminum nanostructures, which faces similar difficulties in nanofabrication as can be seen from the SEM images in **Figure 1d,e**. Unfortunately, the same technique of dissociating the unstable oxide does not work for aluminum due to the high stability of aluminum oxide up to much higher temperatures compared to silver oxide. However, silver oxide is cubic in crystalline geometry and silver and aluminum are themselves face centered cubic with very little lattice mismatch (<1%) between them.^[35] Thus, they are reasonably amicable materials for combined growth and below it is showed that dissociated silver oxide can also serve as an activation layer to reduce aluminum nucleation at early growth state, as is the case for silver deposition described above. Furthermore, the UV plasmonic characteristics of silver and aluminum are similar, with aluminum suffering interband transition induced losses at similar wavelengths as silver. A very thin layer (1 nm) of silver oxide can be used to take advantage of this as was done in the case of silver nanofabrication. However, the residual gases, especially O_2 and H_2O have a strong influence on the aluminum growth process and consequently on the morphology of the deposits.^[36] Especially the dissociative adsorption of H_2O leads to the formation of an oxide–hydroxide phase which alters the growth of the aluminum film. H_2O is present in abundance in the chamber as well as on the substrate and is therefore one of the main constituents in the evaporation unit. Due to strong adsorption of H_2O on oxide surfaces, even its partial removal is challenging and therefore the presence of H_2O must be minimized as far as possible for every process step. To this end, water from the substrate was first removed by baking the substrate at 60 °C for 24 h prior spin-coating of the resist. In the second step, water was removed by baking the substrate plus the resist at 60 °C for about 10 h with periodic introduction of nitrogen into the baking chamber to dry it. The baking temperature was set to 60 °C because of the PMMA, already spin-coated and structured, alters its mechanical properties at higher temperatures.^[37] The steps thereafter until the metal evaporation are

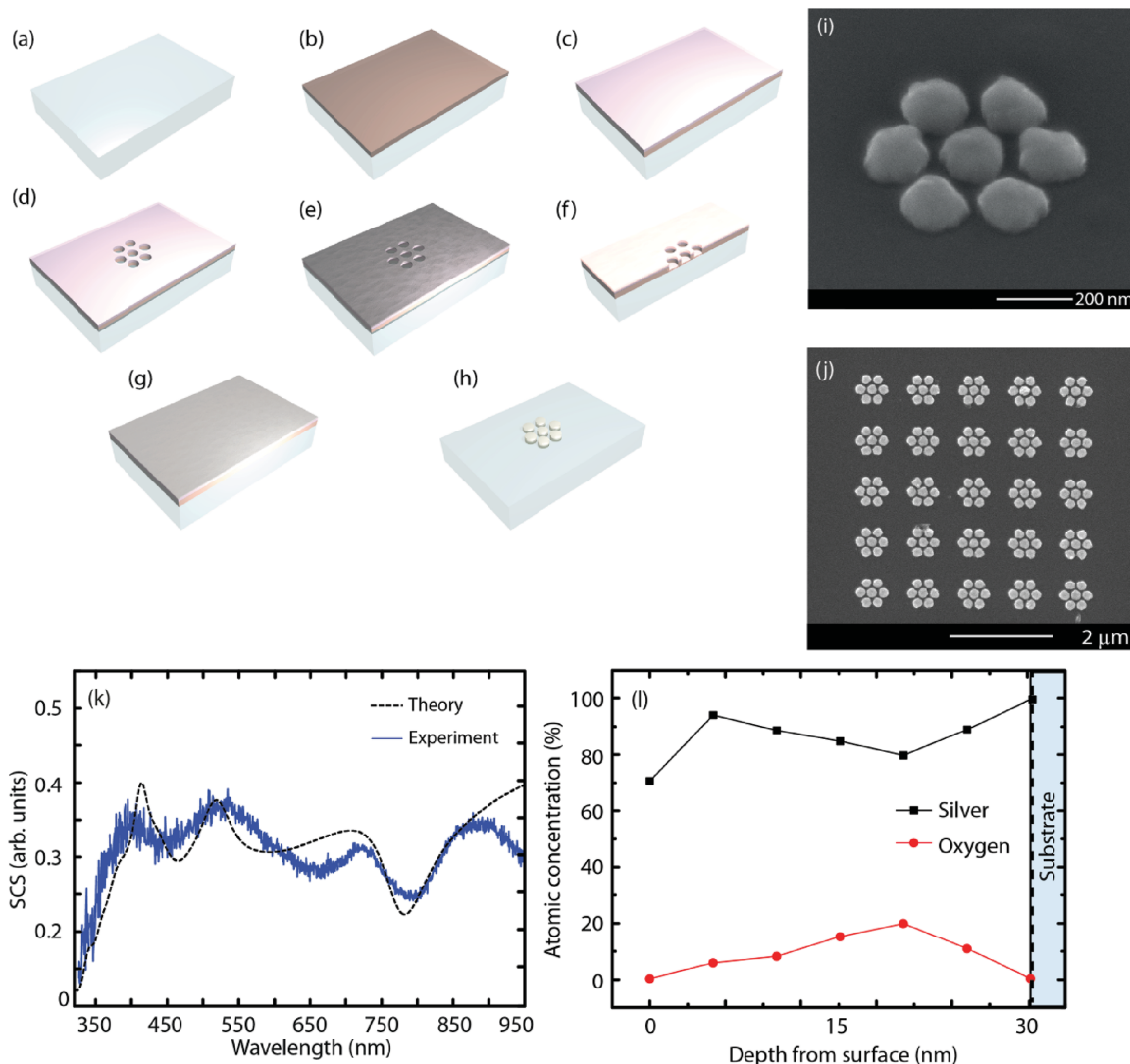


Figure 2. Schematic representation of the process steps of silver heptamers representing: a) The glass substrate, b) the first coating consisting of 120 nm of PMMA 495 kDa, c) the second coating consisting of 60 nm of PMMA 950 kDa, d) e-beam lithography, e) coating of 1 nm of silver oxide, f) cross-section of the wafer showing the dissociation of the oxide thereby providing an activated surface, g) deposition of the silver top layer (30 nm), leading to a smooth surface and h) the liftoff step giving excellent quality of silver heptamers on the substrate, i,j) show SEM images of the heptamers fabricated using the improved recipe, k) scattering measurements of a single silver heptamer showing the good match between simulations and obtained experimental optical properties, l) XPS measurements to chemically characterize the metal composition.

the same as previously described for silver. However, after the initial evaporation of 1 nm of silver oxide, the evaporation chamber was pumped out for 9 h to ensure that oxygen and water are removed as far as possible (typical residual pressure $\approx 5 \times 10^{-7}$ mbar). Thereafter, aluminum was evaporated at 0.1 \AA s^{-1} in three deposition steps, interrupting the process twice for 550 s to let the substrate cool down. This yielded aluminum nanostructures with reproducible gaps down to 10 nm. A schematic of the entire process is shown in Figure 3a–i. To the best of our knowledge, earlier work on aluminum has always involved single piece structures,^[37] which are simpler to fabricate. The recipe involving multiple piece nanostructures in aluminum is therefore an important tool. SEM images of the fabricated nanostructures are shown in Figure 3j,k. It should be noted in Figure 3j that the top aluminum surface still exhibits some roughness, caused by the morphological growth of the metal; however, the lateral features of this double resonance antenna are now very well defined, compared with Figure 1d,e. Those lateral features determine the optical response of the antenna. The optical scattering measurements on the structures, shown

in Figure 3l, exhibit a good match between experiment and simulation, confirming the good optical quality of the aluminum nanostructures. The optical constants applied for the simulations were taken from the literature.^[38] The chemical composition of the fabricated structures was determined using XPS measurements on a film deposited by this technique, as seen in Figure 3m and shows a very uniform distribution of silver throughout the depth of the structure, indicating the formation of an alloy-like material which may be attributed to diffusion due to the small lattice mismatch of aluminum and silver.^[39] The presence of oxygen in the bulk of the structure is also seen to be lower than at the top and bottom surfaces (note that the XPS measurements reported in Figure 3m were performed at a higher etching rate than for Figure 2l and eroded the substrate). The ease with which silver and aluminum seem to interact confirms the amicability between the two metals vis-à-vis nanofabrication. Furthermore, the presence of silver has a minimal impact on the optical properties of the aluminum nanostructures.

Spectroscopic ellipsometry was carried out using a SOPRA GSE 5E spectroscopic ellipsometer for 150 nm thick silver and aluminum

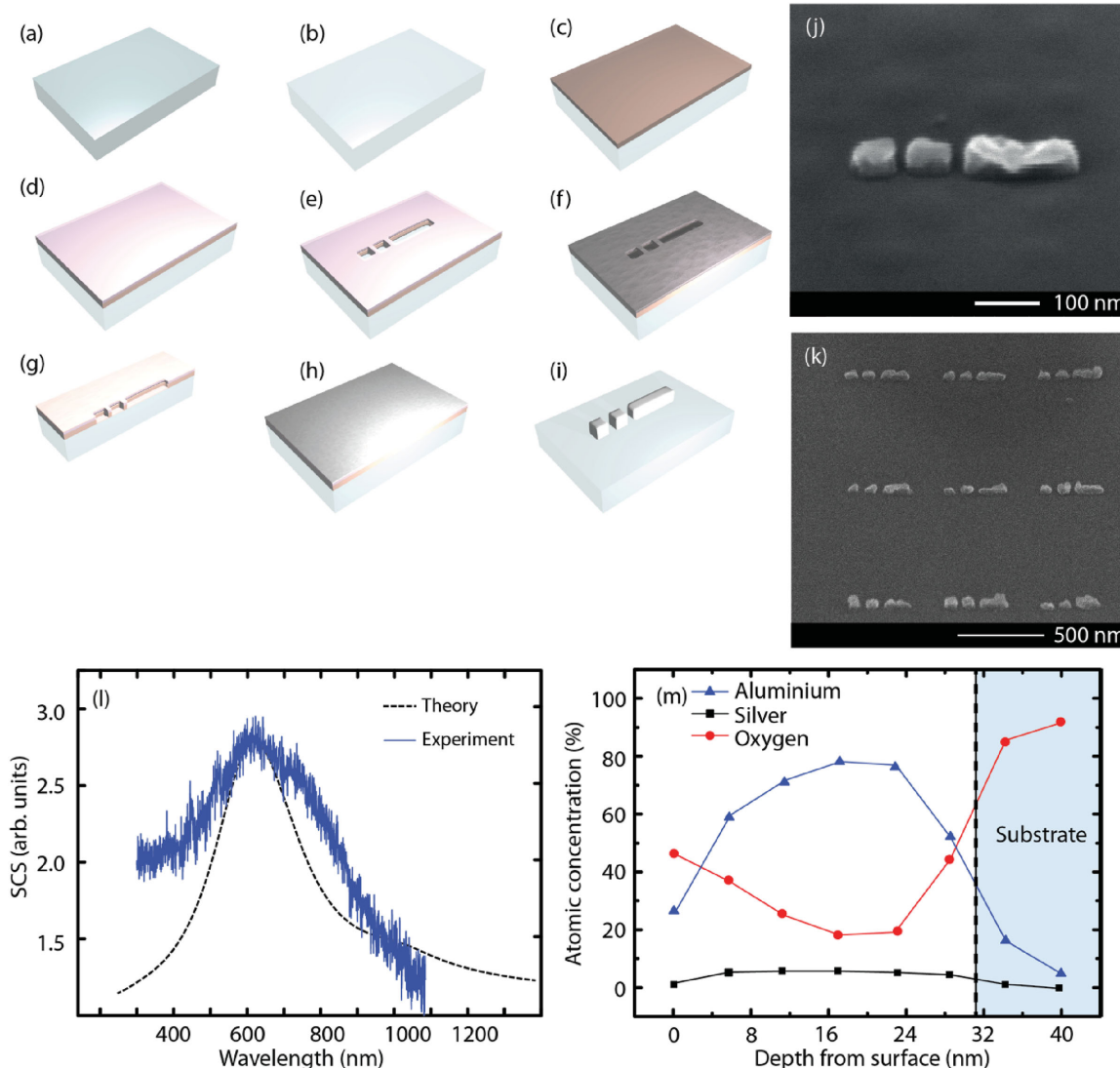


Figure 3. Schematic representation of the process steps during the fabrication of aluminum double resonance antennas (DRA) representing: a) The glass substrate before heating, b) the glass substrate after heating to remove water, c) the first coating consisting of 120 nm of PMMA 495 kDa, d) the second coating consisting of 60 nm of PMMA 950 kDa, e) e-beam lithography process to write the DRA structures, f) coating of 1 nm of silver oxide, g) cross-section of the wafer showing dissociation of the oxide thereby providing an activated surface, h) deposition of aluminum (30 nm) on top, leading to a smooth surface and the lift-off step giving excellent quality of aluminum DRA structures, j,k) show SEM images of the DRA fabricated with the improved recipe, l) scattering measurements of a single aluminum DRA showing the good match between simulations and obtained experimental optical properties, and m) XPS measurements to chemically characterize the metal composition.

films deposited according to the processes described above. For all measurements, the angle of the incident light was set to 75° and the numerical data analysis was carried out using the WINELLI II software. For the silver film, the real and imaginary parts (ϵ_r and ϵ_i , respectively) of the dielectric function determined from the amplitude component Ψ and the phase difference Δ are in relatively good agreement with the values given by Johnson and Christy,^[34] with however a larger imaginary part ϵ_i . Measured and literature values for ϵ_r and ϵ_i are shown in **Figure 4a**. The dielectric functions for aluminum from the measurements and the literature,^[38] are shown in **Figure 4b**. The discrepancy between the two is larger than for silver. For aluminum, the measured dielectric function can be approximated using a Drude model with additional Lorentz oscillators mimicking the interband transitions. This approach reveals a decrease of the plasma frequency from $\omega_p = 2.4 \times 10^{16} \text{ s}^{-1}$, reported in the literature,^[40] to $\omega_p = 2.1 \times 10^{16} \text{ s}^{-1}$ for the ellipsometry data. Moreover, the interband transition at $\lambda_0 = 800 \text{ nm}$ ^[41] as reported in the

literature slightly shifted to 790 nm in the measurements. The complete ellipsometry data for silver and aluminum are given in the Supporting Information.

In summary, a new recipe for high yield and high quality fabrication of lithographic nanostructures in silver and aluminum with intended applications in plasmonics was developed and demonstrated. In order to reduce grain sizes of the metal deposits, a thin layer of silver oxide was first deposited. The latter dissociated under vacuum conditions providing a seed layer which enabled enhanced nucleation of silver and aluminum, leading to smaller grain sizes. The good agreement in the linear optical properties of the structures between the experimental results and simulations showed that the optical properties of the fabricated nanostructures are very good which is, additionally, supported by ellipsometry measurements. The clean fabrication of reproducible features down to 10 nm makes this new recipe very attractive for diverse applications, especially for nonlinear and UV plasmonics. Indeed, it is

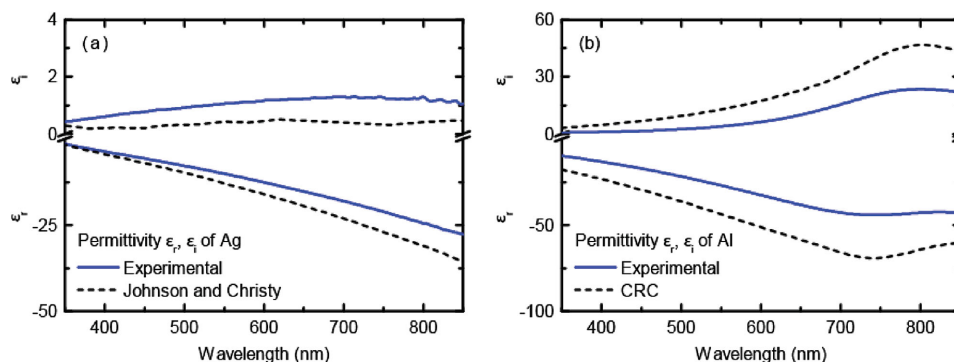


Figure 4. Dielectric functions measured by ellipsometry for a 150 nm thick film made of a) silver and b) aluminum using the recipe presented in this Communication. The experimental data are compared to the literature data from ref. [34] for silver and from ref. [38] for aluminum.

known that for second harmonic generation, the nonlinear signal is generated at the surface of the metal,^[42] and is dramatically influenced by surface roughness.^[43] Comparing for example Figure 1a–c with Figure 2i,j, one clearly sees that the role of the different geometrical features (particle size, gap size, arrangement of the particles) on the nonlinear response of the silver heptamer will be much easier to study using well defined structures fabricated with the new recipe (Figure 2) compared to the original, ill-defined geometries shown in Figure 1.

Supporting Information

Supporting Information is available from the Wiley Online Library or from the author.

Acknowledgements

K.T. and Ch.S. contributed equally to this work. The authors are grateful to Philippe Flückiger for his support of the project. Support from Nicolas Xanthopoulos with the XPS measurements and Robert D. Wolke with the artwork, as well as funding from the Swiss National Science Foundation (Projects 200021_132694 and 200020_153662) are gratefully acknowledged.

Received: December 10, 2015
Published online: March 15, 2016

- [1] S. A. Maier, *Plasmonics: Fundamentals and Applications*, Springer, New York 2007.
- [2] P. R. West, S. Ishii, G. V. Naik, N. K. Emani, V. M. Shalae, A. Boltasseva, *Laser Photonics Rev.* **2010**, *4*, 795.
- [3] W. H. Zhang, H. Fischer, T. Schmid, R. Zenobi, O. J. F. Martin, *J. Phys. Chem. C* **2009**, *113*, 14672.
- [4] P. Berini, I. De Leon, *Nat. Photonics* **2012**, *6*, 16.
- [5] a) B. Gallinet, T. Siegfried, H. Sigg, P. Nordlander, O. J. F. Martin, *Nano Lett.* **2013**, *13*, 497; b) M. Piliarik, H. Sipova, P. Kvasnicka, N. Galler, J. R. Krenn, J. Homola, *Opt. Express* **2012**, *20*, 672.
- [6] N. J. Halas, S. Lal, W. S. Chang, S. Link, P. Nordlander, *Chem. Rev.* **2011**, *111*, 3913.
- [7] a) L. Huang, S. J. Maerkl, O. J. F. Martin, *Opt. Express* **2009**, *17*, 6018; b) W. H. Zhang, L. N. Huang, C. Santschi, O. J. F. Martin, *Nano Lett.* **2010**, *10*, 1006.
- [8] M. W. Knight, H. Sobhani, P. Nordlander, N. J. Halas, *Science* **2011**, *332*, 702.
- [9] R. W. Boyd, *Nonlinear Optics*, Academic Press, New York 2008.
- [10] a) J. B. Khurgin, G. Sun, *Opt. Express* **2012**, *20*, 28717; b) K. Thyagarajan, S. Rivier, A. Lovera, O. J. F. Martin, *Opt. Express* **2012**, *20*, 12860; c) V. K. Valev, *Langmuir* **2012**, *28*, 15454; d) R. Czaplicki, H. Husu, R. Siikanen, J. Makitalo, M. Kauranen, J. Laukkanen, J. Lehtolahti, M. Kuittinen, *Phys. Rev. Lett.* **2013**, *110*, 093902; e) K. Thyagarajan, J. Butet, O. J. F. Martin, *Nano Lett.* **2013**, *13*, 1847; f) J. Butet, P.-F. Brevet, O. J. F. Martin, *ACS Nano* **2015**, *9*, 10545.
- [11] a) E. A. Mamonov, T. V. Murzina, I. A. Kolmychek, A. I. Maydykovsky, V. K. Valev, A. V. Silhanek, T. Verbiest, V. V. Moshchalkov, O. A. Aktsipetrov, *Opt. Express* **2012**, *20*, 8518; b) V. K. Valev, X. Zheng, C. G. Biris, A. V. Silhanek, V. Volskiy, B. De Clercq, O. A. Aktsipetrov, M. Ameloot, N. C. Panoiu, G. A. E. Vandenbosch, V. V. Moshchalkov, *Opt. Mater. Express* **2011**, *1*, 36.
- [12] M. Castro-Lopez, D. Brinks, R. Sapienza, N. F. van Hulst, *Nano Lett.* **2011**, *11*, 4674.
- [13] a) G. Bautista, M. J. Huttunen, J. M. Kontio, J. Simonen, M. Kauranen, *Opt. Express* **2013**, *21*, 21918; b) M. Hentschel, T. Utikal, H. Giessen, M. Lippitz, *Nano Lett.* **2012**, *12*, 3778; c) J. B. Khurgin, G. Sun, *Opt. Express* **2013**, *21*, 27460.
- [14] S. Kim, J. H. Jin, Y. J. Kim, I. Y. Park, Y. Kim, S. W. Kim, *Nature* **2008**, *453*, 757.
- [15] T. Hanke, J. Cesar, V. Knittel, A. Trugler, U. Hohenester, A. Leitenstorfer, R. Bratschitsch, *Nano Lett.* **2012**, *12*, 992.
- [16] M. Danckwerts, L. Novotny, *Phys. Rev. Lett.* **2007**, *98*, 026104.
- [17] M. Kauranen, A. V. Zayats, *Nat. Photonics* **2012**, *6*, 737.
- [18] J. M. McMahon, G. C. Schatz, S. K. Gray, *Phys. Chem. Chem. Phys.* **2013**, *15*, 5415.
- [19] Y. Yang, J. M. Callahan, T. H. Kim, A. S. Brown, H. O. Everitt, *Nano Lett.* **2013**, *13*, 2837.
- [20] R. Mupparapu, K. Vynck, I. Malfanti, S. Vignolini, M. Burrelli, P. Scudo, R. Fusco, D. S. Wiersma, *Opt. Lett.* **2012**, *37*, 368.
- [21] G. Maidecchi, G. Gonella, R. P. Zaccaria, R. Moroni, L. Anghinolfi, A. Giglia, S. Nannarone, L. Mattered, H. L. Dai, M. Canepa, F. Bisio, *ACS Nano* **2013**, *7*, 5834.
- [22] S. Butun, N. A. Cinel, E. Ozbay, *Opt. Express* **2012**, *20*, 2649.
- [23] X. D. Yang, J. Yao, J. Rho, X. B. Yin, X. Zhang, *Nat. Photonics* **2012**, *6*, 450.
- [24] J. Olson, A. Manjavacas, L. Liu, W.-S. Chang, B. Foerster, N. S. King, M. W. Knight, P. Nordlander, N. J. Halas, S. Link, *Proc. Natl. Acad. Sci. USA* **2014**, *111*, 14348.
- [25] a) H. Liu, J. Teng, *J. Mol. Eng. Mater.* **2013**, *01*, 1250005; b) O. J. F. Martin, *Microelectron. Eng.* **2003**, *67–68*, 24.
- [26] a) M. W. Knight, N. S. King, L. F. Liu, H. O. Everitt, P. Nordlander, N. J. Halas, *ACS Nano* **2014**, *8*, 834; b) M. W. Knight, L. F. Liu, Y. M. Wang, L. Brown, S. Mukherjee, N. S. King, H. O. Everitt, P. Nordlander, N. J. Halas, *Nano Lett.* **2012**, *12*, 6000; c) P. M. Schwab,

- C. Moosmann, M. D. Wissert, E. W. G. Schmidt, K. S. Ilin, M. Siegel, U. Lemmer, H. J. Eisler, *Nano Lett.* **2013**, *13*, 1535.
- [27] O. J. F. Martin, M. Paulus, *J. Microsc. Oxford* **2002**, *205*, 147.
- [28] a) N. Formica, D. S. Ghosh, A. Carrilero, T. L. Chen, R. E. Simpson, V. Pruneri, *ACS Appl. Mater. Interfaces* **2013**, *5*, 3048; b) H. Liu, B. Wang, E. S. P. Leong, P. Yang, Y. Zong, G. Y. Si, J. H. Teng, S. A. Maier, *ACS Nano* **2010**, *4*, 3139; c) V. J. Logeeswaran, N. P. Kobayashi, M. S. Islam, W. Wu, P. Chaturvedi, N. X. Fang, S. Y. Wang, R. S. Williams, *Nano Lett.* **2008**, *9*, 178.
- [29] C. T. Campbell, *Surf. Sci. Rep.* **1997**, *27*, 1.
- [30] a) A. F. Benton, L. C. Drake, *J. Am. Chem. Soc.* **1932**, *54*, 2186; b) W. E. Garner, L. W. Reeves, *Trans. Faraday Soc.* **1954**, *50*, 254; c) B. V. L'Vov, *Thermochim. Acta* **1999**, *333*, 13.
- [31] Y. H. Kim, R. O. Suzuki, H. Numakura, H. Wada, K. Ono, *J. Alloys Compd.* **1997**, *248*, 251.
- [32] G. B. Schaffer, B. J. Hall, *Metall. Mater. Trans. A* **2002**, *33*, 3279.
- [33] a) B. Gallinet, A. M. Kern, O. J. F. Martin, *J. Opt. Soc. Am. A-Opt. Image Sci. Vision* **2010**, *27*, 2261; b) B. Gallinet, O. J. F. Martin, *ACS Nano* **2011**, *5*, 8999.
- [34] P. B. Johnson, R. W. Christy, *Phys. Rev. B* **1972**, *6*, 4370.
- [35] a) L. Liu, W. A. Bassett, *J. Appl. Phys.* **1973**, *44*, 1475; b) W. Witt, *Z. Naturforsch., A: Astrophys., Phys. Phys. Chem.* **1967**, *A 22*, 92.
- [36] a) Y. Chiba, Y. Abe, M. Kawamura, K. Sasaki, *Vacuum* **2008**, *83*, 483; b) M. J. Verkerk, W. Brankaert, *Thin Solid Films* **1986**, *139*, 77.
- [37] M. Dixit, S. Gupta, V. Mathur, K. S. Rathore, K. Sharma, N. S. Saxena, *Chalcogenide Lett.* **2009**, *6*, 131.
- [38] E. D. Palik, *Handbook of Optical Constants of Solids*, Academic Press, New York **1985**.
- [39] N. W. Ashcroft, N. D. Mermin, *Solid State Physics*, Cengage Learning, New York **1976**.
- [40] J. Jung, J. Bork, T. Holmgaard, N. A. Kortbek, K. Pedersen, *Semester Project*, Aalborg University (Denmark) **2004**.
- [41] R. Wilks, R. J. Hicken, *J. Phys.-Condens. Matter* **2004**, *16*, 4607.
- [42] G. Bachelier, J. Butet, I. Russier-Antoine, C. Jonin, E. Benichou, P.-F. Brevet, *Phys. Rev. B* **2010**, *82*, 235403.
- [43] J. Butet, K. Thyagarajan, O. J. F. Martin, *Nano Lett.* **2013**, *13*, 1787.